

# In vivo RNA editing of point mutations via RNA-guided adenosine deaminases

Dhruva Katrekar<sup>1</sup>, Genghao Chen<sup>1</sup>, Dario Meluzzi<sup>1</sup> , Ashwin Ganesh<sup>1</sup>, Atharv Worlikar<sup>1</sup>, Yu-Ru Shih<sup>1,2</sup>, Shyni Varghese<sup>1,2</sup> and Prashant Mali<sup>1</sup> \*

**We present in vivo sequence-specific RNA base editing via adenosine deaminases acting on RNA (ADAR) enzymes with associated ADAR guide RNAs (adRNAs). To achieve this, we systematically engineered adRNAs to harness ADARs, and comprehensively evaluated the specificity and activity of the toolsets in vitro and in vivo via two mouse models of human disease. We anticipate that this platform will enable tunable and reversible engineering of cellular RNAs for diverse applications.**

Adenosine-to-inosine RNA editing, a common post-transcriptional RNA modification, is catalyzed by ADAR enzymes<sup>1</sup>. Inosine is a deaminated form of adenosine that is biochemically recognized as guanine. Recently, multiple studies have demonstrated ADAR-mediated targeted RNA editing<sup>2–9</sup>. Building on these, we engineered and optimized two orthogonal toolsets for sequence-specific programmable RNA base editing in vitro and in vivo. Specifically, we used a system for targeted RNA editing via ADAR1/2 with associated adRNAs (Fig. 1a). The adRNAs comprise in part a programmable antisense region that is complementary to the target RNA sequence with a mismatched cytidine opposite the target adenosine. Additionally, in one version they bear zero, one or two ADAR-recruiting domains engineered from the naturally occurring ADAR substrate GluR2 pre-messenger RNA (pre-mRNA) (per refs. <sup>3,4</sup> and referred to forthwith as GluR2 adRNA), and in a second format they include two MS2 hairpins flanking the antisense region (referred to forthwith as MS2 adRNA). The GluR2 adRNA was systematically optimized to enhance recruitment of exogenous and/or endogenous ADARs through the evaluation of multiple scaffold variants, including mutagenized scaffolds based on guanine–cytosine (G–C) versus adenosine–uracil (A–U) pairing, the addition of editing inducer elements<sup>10</sup>, and antisense domain length<sup>11</sup> and mismatch position modifications (Fig. 1b, Supplementary Figs. 1 and 2). The latter MS2 adRNA version was in turn optimized to harness synthetic proteins comprising the deaminase domains of ADAR1 or ADAR2 fused to the MS2 coat protein (MCP), via systematic antisense domain length and mismatch position modifications, coupled with the use of hyperactive versions of the deaminase domains, and versions bearing nuclear localization signal (NLS) or nuclear export signal (NES) (Fig. 1b and Supplementary Figs. 3a and 4a).

We comprehensively evaluated the activity of the two systems above in vitro, and also benchmarked it with the recently developed RNA editing system based on Cas13b<sup>7</sup>. We observed the following: (1) the engineered constructs were active in their ability to effect targeted RNA editing, with yields comparable to those of the Cas13b-based system (Fig. 1b, Supplementary Fig. 4a and Supplementary Tables 1 and 2), and U6-transcribed adRNAs and chemically

synthesized adRNAs were both an effective format (Supplementary Fig. 4). (2) adRNAs bearing long antisense domains, both with and without GluR2 domains, sufficed to recruit exogenously expressed ADARs and, to a degree, endogenous ADARs<sup>12</sup> to enable efficient RNA editing (Fig. 1b and Supplementary Figs. 2b and 5). (3) The constructs based on the MS2 adRNAs and corresponding MCP–ADAR1/2 fusions showed robust activity, including across a large panel of endogenous genes chosen along a spectrum of different expression levels (Fig. 1b and Supplementary Figs. 4a and 5). (4) The use of NES and/or hyperactive deaminase domains in the MCP–ADAR1/2 fusions consistently yielded higher RNA editing yields at the target adenosine, but also led to a higher propensity toward editing at nontargeted adenosines in the flanking sequences (Fig. 1b and Supplementary Figs. 4a and 6a). To further validate this, we showed that a similar promiscuity ensued also from deletion of the native NLS domain in ADAR2 ( $\Delta$ 1–138)<sup>13</sup>, as well as from its hyperactive mutant ADAR2 (E488Q) (Supplementary Fig. 6b–d). (5) These two toolsets were operationally orthogonal when we used adRNAs with short antisense domains: specifically, we evaluated the editing efficiency of the MCP–ADAR2 deaminase domain fusion with a co-expressed MS2 adRNA or GluR2 adRNA and observed on-target editing only via the former. Conversely, we also confirmed that full-length ADAR2 was recruited by GluR2 adRNA and not the MS2 adRNAs (Supplementary Fig. 3b).

Having demonstrated the robust activity of this toolset, we next investigated its specificity profiles via analysis of the transcriptome-wide off-target A>G editing effected by this system (Fig. 1c). To this end, HEK293T cells were transfected with each construct and analyzed by RNA sequencing (RNA-seq). Untransfected cells were included as controls. From each sample, we collected ~40 million uniquely aligned sequencing reads. We then used Fisher's exact test to quantify significant changes in A>G editing yields, relative to untransfected cells, at each reference adenosine site having sufficient read coverage. The number of sites with at least one A>G editing event detected in any of the samples was computed. Of these, the number of sites with statistically significant A>G edits, at a false discovery rate (FDR) of 1% and with fold change of at least 1.1, was found to vary over a wide range, from lowest for the MCP–ADAR2 DD–NLS construct to highest for MCP–ADAR1 DD (E1008Q)–NES (Supplementary Figs. 7–9 and Supplementary Tables 3 and 4). To investigate the distribution of editing yields, we generated violin plots considering the A sites whose editing yields changed significantly in at least one sample (Fig. 1c). Taken together, our RNA-seq experiments revealed that transcriptome-wide off-target edits were (1) less prevalent in MCP–ADAR constructs with NLS than in constructs with NES; (2) less prevalent in MCP–ADAR2

<sup>1</sup>Department of Bioengineering, University of California, San Diego, CA, USA. <sup>2</sup>Present address: Department of Biomedical Engineering, Duke University, Durham, NC, USA. \*e-mail: [pmali@ucsd.edu](mailto:pmali@ucsd.edu)

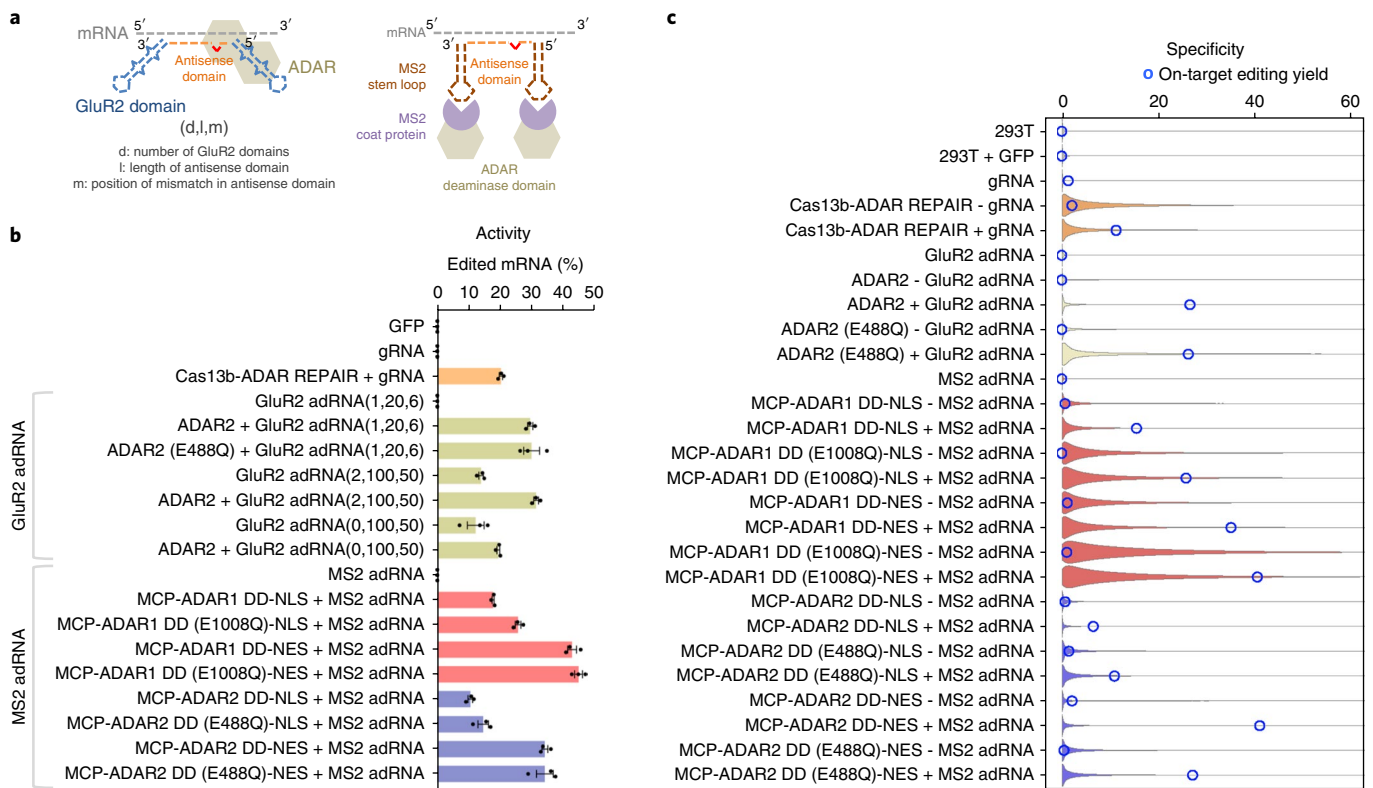


**Fig. 1 | Engineering programmable RNA editing and characterizing specificity profiles.** **a**, Schematics of RNA editing via constructs using the full-length ADAR2 and an engineered adRNA derived from the GluR2 transcript, or MCP fusions to the ADAR1/2 deaminase domains and the corresponding MS2 hairpin bearing adRNA. **b**, Comparison of RNA editing efficiency of the endogenous RAB7A transcript by different RNA editing constructs quantified by Sanger sequencing (efficiency calculated as the ratio of Sanger peak heights G/(A + G)). Experiments were carried out on human embryonic kidney (HEK) 293T cells. Values represent mean  $\pm$  s.e.m. ( $n = 3$ ). **c**, Violin plots representing distribution of A>G editing yields observed at reference sites where at least one treatment sample was found to have a significant change (Fisher's exact test, FDR = 1%) in editing yield relative to the control sample. Blue circles indicate editing yields at the target A site within the RAB7A transcript. To better visualize the shapes of the distributions, their maximum extent along the y axis was equalized across all plots and they were truncated at 60% yield.

constructs than in MCP-ADAR1 constructs; (3) less prevalent in the wild-type MCP-ADAR constructs than in the E>Q hyperactive mutants (Supplementary Fig. 8 and Supplementary Table 4); and (4) primarily due to ADAR overexpression. In addition, the use of long-antisense-domain adRNAs alone to effect on-target editing resulted in the fewest off-targets (Supplementary Fig. 9).

Following these in vitro studies, we next evaluated this system for in vivo RNA-targeting applications using the adRNA with exogenous ADAR expression construct versions, as these consistently enabled the highest in vitro RNA editing yields. We focused first on the *mdx* mouse model for Duchenne muscular dystrophy (DMD), which bears an ochre stop site in exon 23 of the dystrophin gene. This choice was additionally motivated by the fact that nonsense mutations in general are responsible for nearly 11% of all gene lesions described as causing inheritable human disease, and close to 20% of disease-associated single-base substitutions that affect the coding regions of genes<sup>14</sup>. Thus, validation of an RNA editing strategy here would have broad therapeutic application. Toward this, we first optimized RNA editing of stop codons in vitro (Supplementary Fig. 10a,b). Notably, we observed that the addition of a second copy of adRNA significantly improved the targeting efficiencies (Supplementary Fig. 10c), and thus in all our in vivo studies we used a dual-adRNA delivery approach. To test the effectiveness of our system in editing the premature stop codon in *mdx* dystrophin mRNA, we initially evaluated our constructs in vitro (Supplementary Fig. 10d). We next packaged our constructs into adenovirus-associated 8 (AAV8), and injected  $2 \times 10^{12}$  vector genomes per muscle into the

tibialis anterior or gastrocnemius muscle of *mdx* mice. To further benchmark our approach, we concurrently also targeted *mdx* mice via CRISPR-Cas9-based excision of exon 23<sup>15-17</sup> (Fig. 2a). Four or eight weeks after the injection, tibialis anterior and gastrocnemius muscles were collected from *mdx* mice, wild-type mice, and mice treated with adRNA targeting and non-targeting controls and with CRISPR-Cas9. Immunofluorescence staining revealed clear restoration of dystrophin expression via targeted RNA editing (Fig. 2b and Supplementary Fig. 11a). In addition, neuronal nitric oxide synthase (nNOS) localization was also restored at the sarcolemma (Fig. 2b and Supplementary Fig. 11a). RNA editing yields (TAA>TGG/TAG/TGA) of up to 3.6% and TAA>TGG of up to 2.4% were observed in treated mice (Fig. 2c and Supplementary Fig. 10e). Immunoblots of the treated muscles confirmed the immunofluorescence observations, demonstrating 1–2.5% protein restoration (Supplementary Fig. 11b). As a benchmark, muscles injected with vectors bearing CRISPR-Cas9 also expectedly led to restoration of dystrophin expression in a subset of the muscle cells (Fig. 2b), with immunoblots of the treated muscles confirming up to 10% protein restoration (Supplementary Fig. 11c).

To further confirm the efficacy of this approach, we next evaluated ADAR-mediated RNA editing in an independent mouse model of human disease, the male sparse fur ash (*spf<sup>fish</sup>*) model of ornithine transcarbamylase (OTC) deficiency. This *spf<sup>fish</sup>* mouse model harbors a G>A point mutation in the last nucleotide of the fourth exon of the OTC gene, which leads to OTC mRNA deficiency and production of a mutant protein<sup>18</sup>. Recent studies have demonstrated

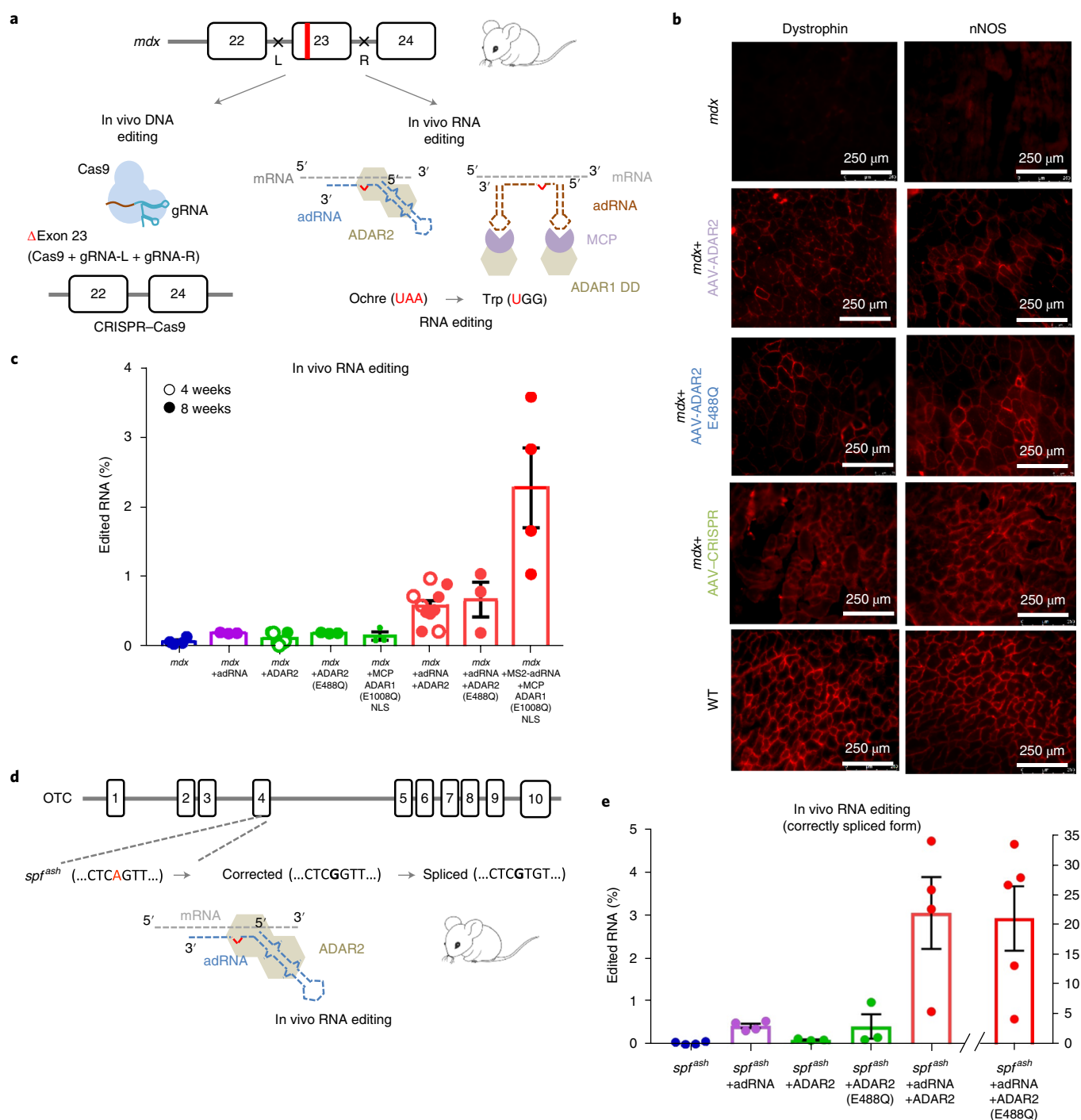


**Fig. 2 | In vivo RNA editing in mouse models of human disease. a**, Schematic of the DNA and RNA targeting approaches used to restore dystrophin expression in the *mdx* mouse model of DMD: (left) a dual gRNA–CRISPR-based approach leading to in-frame excision of exon 23, and (right) ADAR2- and MCP–ADAR1-based editing of the ochre codon. **b**, Immunofluorescence staining for dystrophin in the tibialis anterior muscle after intramuscular injection of the indicated constructs (scale bar, 250  $\mu$ m). **c**, In vivo TAA>TGG/TAG/TGA RNA editing efficiencies in corresponding treated adult *mdx* mice. Values represent mean  $\pm$  s.e.m. ( $n = 4, 3, 7, 3, 10, 3$  and 4 independent tibialis anterior muscles, respectively). **d**, Schematic of the OTC locus in the *spf<sup>ash</sup>* mouse model of OTC deficiency, which has a G>A point mutation at a donor splice site in the last nucleotide of exon 4, and approach for correction of mutant OTC mRNA via ADAR2-mediated RNA editing. **e**, In vivo RNA correction efficiencies in correctly spliced OTC mRNA in the livers of treated adult *spf<sup>ash</sup>* mice (retro-orbital injections of AAV8–ADAR2 and AAV8–ADAR2 (E488Q)). Values represent mean  $\pm$  s.e.m. ( $n = 4, 4, 3, 3, 4$  and 5 independent animals, respectively).

the use of CRISPR–Cas9 and homologous-recombination-based strategies for robust correction of this mutation in neonatal mice<sup>19</sup>. To test the effectiveness of our system in editing the point mutation in *spf<sup>ash</sup>* OTC mRNA (Fig. 2d), we initially evaluated our constructs

in vitro (Supplementary Fig. 12a). We next packaged our constructs into AAV8, which has high liver tropism<sup>19</sup>, and injected  $2.5 \times 10^{12}$  vector genomes per mouse in 10–12-week-old *spf<sup>ash</sup>* mice. Three to four weeks post-injection, we collected liver samples from *spf<sup>ash</sup>*

mice, wild-type littermates and *spf<sup>ash</sup>* mice treated with the ADAR2 targeting and non-targeting vectors and evaluated corresponding editing efficiency via NGS. Notably, after the delivery of adRNA and ADAR2, we observed 0.8–4.7% edited mRNA among the correctly spliced OTC mRNA, and, notably, adRNA alone resulted in low but significant RNA editing yields (Fig. 2e and Methods). Moreover, after the delivery of the hyperactive ADAR2 mutant (E488Q), we observed a high edited fraction (4.6–33.8%) in the correctly spliced OTC mRNA (Fig. 2e and Supplementary Fig. 12b) and 4.6–8.2% in the OTC pre-mRNA (Supplementary Fig. 12c), and confirmed a reduction in the incorrectly spliced product (Supplementary Fig. 12d). Immunoblots of the treated liver samples confirmed partial (2.5–5%) restoration of OTC protein (Supplementary Fig. 12e).

Taken together, our results establish the utility of RNA-guided ADARs for in vivo RNA editing of point mutations. Moving forward, we note that sequence preferences of the ADAR enzymes, tissue-specific regulators of RNA editing, RNA folding, intrinsic half-life, localization, translation machinery<sup>9</sup> and resident RNA-binding proteins can potentially affect the accessibility and editability of target sites in the RNA, and will be important design parameters to consider for efficacious targeting. For instance, in the *mdx* model, ADAR-based RNA editing approaches have to compete with nonsense-mediated decay of mutant dystrophin mRNA, and also the requirement for effecting two A>I substitutions in the context of non-ideal flanking nucleotides to eliminate the premature stop codon and potential effects on RNA stability and function. Furthermore, in the *spf<sup>ash</sup>* model, the need to target the transient OTC pre-mRNA entails rapid target engagement and editing. Further progress will also require addressing of important limitations of the system such as the off-targets induced by intrinsic enzyme–RNA binding, processivity, promiscuity, stimulation of the interferon response by the delivery modalities per se (such as lipid, nanoparticles or viral vectors) leading in turn to potentially altered endogenous ADAR expression, the potential of adRNAs to induce RNA interference (Supplementary Fig. 13) and also off-target hybridization of the antisense domain of the adRNA, which could potentially have deleterious effects<sup>20</sup>. In this regard, our studies revealed toxicity in mice systemically injected with the hyperactive ADAR mutants (Supplementary Fig. 14). While we hypothesize that off-target RNA editing due to the hyperactive version may be responsible for the observed negative effects on mouse health, additional work needs to be performed to ascertain the underlying mechanisms. These studies will be critical to aid systematic improvement in the specificity and safety of this approach. Another important consideration while considering RNA targeting for gene therapy, especially via the use of non-integrating vectors, is the necessity for periodic readministration of the effector constructs owing to the typically limited half-life of edited mRNAs and effectors. In this regard, compared to CRISPR-based RNA editing approaches, the RNA-guided ADAR strategy is directly relevant to human therapeutics because versions of this toolset solely utilize effector RNAs and human proteins. Additionally, as ADARs are widely expressed—for instance, ADAR1 across most human tissues and ADAR2 in particular in the lung and brain—endogenous recruitment of these via adRNAs bearing long-antisense domains (as demonstrated in Figs. 1b and 2e and Supplementary Figs. 2b and 5) presents a very attractive strategy for efficacious RNA editing. We thus anticipate that with progressive improvements, this toolset will have broad implications for diverse basic science and therapeutic applications.

## Online content

Any methods, additional references, Nature Research reporting summaries, source data, statements of data availability and associated accession codes are available at <https://doi.org/10.1038/s41592-019-0323-0>.

Received: 16 August 2018; Accepted: 13 December 2018;  
Published online: 8 February 2019

## References

- Melcher, T. et al. *Nature* **379**, 460–464 (1996).
- Montiel-Gonzalez, M. F., Vallecillo-Viejo, I., Yudowski, G. A. & Rosenthal, J. J. C. *Proc. Natl Acad. Sci. USA* **110**, 18285–18290 (2013).
- Wettengel, J., Reautschnig, P., Geisler, S., Kahle, P. J. & Staffor, T. *Nucleic Acids Res.* **45**, 2797–2808 (2017).
- Fukuda, M. et al. *Sci. Rep.* **7**, 41478 (2017).
- Vallecillo-Viejo, I. C., Liscovitch-Brauer, N., Montiel-Gonzalez, M. F., Eisenberg, E. & Rosenthal, J. J. C. *RNA Biol.* **15**, 104–114 (2018).
- Sinnamon, J. R. et al. *Proc. Natl Acad. Sci. USA* **114**, E9395–E9402 (2017).
- Cox, D. B. T. et al. *Science* **358**, 1019–1027 (2017).
- Azad, M. T. A., Bhakta, S. & Tsukahara, T. *Gene Ther.* **24**, 779–786 (2017).
- Vogel, P. et al. *Nat. Methods* **15**, 535–538 (2018).
- Daniel, C., Widmark, A., Rigardt, D. & Öhman, M. *Genome. Biol.* **18**, 195 (2017).
- Wolf, T. M., Chase, J. M. & Stinchcomb, D. T. *Proc. Natl Acad. Sci. USA* **92**, 8298–8302 (1995).
- Chung, H. et al. *Cell* **172**, 811–824 (2018).
- Desterro, J. M. P. et al. *J. Cell Sci.* **116**, 1805–1818 (2003).
- Mort, M., Ivanov, D., Cooper, D. N. & Chuzhanova, N. A. *Hum. Mutat.* **29**, 1037–1047 (2008).
- Nelson, C. E. et al. *Science* **351**, 403–407 (2016).
- Tabebordbar, M. et al. *Science* **351**, 407–411 (2016).
- Long, C. et al. *Science* **351**, 400–403 (2016).
- Hodges, P. E. & Rosenberg, L. E. *Proc. Natl Acad. Sci. USA* **86**, 4142–4146 (1989).
- Yang, Y. et al. *Nat. Biotechnol.* **34**, 334–338 (2016).
- Chen, L. et al. *Nat. Med.* **19**, 209–216 (2013).

## Acknowledgements

We thank A. Moreno, L. Hodge, D. Zhao, U. Parekh and other members of the Mali laboratory for advice and help with experiments, and the Salk GT3 viral core for help with AAV production. We also thank the UCSD IGM Genomics Center for providing NGS technologies and services. This work was generously supported by the Burroughs Wellcome Fund (no. 1013926 to P.M.) and the National Institutes of Health (grant numbers R01HG009285, RO1CA222826, and RO1GM123313 to P.M., and F32DK112682 to D.M.).

## Author contributions

D.K. and P.M. conceived the study and wrote the paper. D.M. performed computational analyses and wrote the paper. D.K., G.C., A.G., A.W. and P.M. performed experiments. Y.S. and S.V. provided technical advice.

## Competing interests

D.K. and P.M. have filed patents based on this work. P.M. is a scientific co-founder of Navega Therapeutics, Pretzel Therapeutics, Engine Biosciences and Shape Therapeutics. The terms of these arrangements have been reviewed and approved by the University of California, San Diego, in accordance with its conflict-of-interest policies.

## Additional information

Supplementary information is available for this paper at <https://doi.org/10.1038/s41592-019-0323-0>.

Reprints and permissions information is available at [www.nature.com/reprints](http://www.nature.com/reprints).

Correspondence and requests for materials should be addressed to P.M.

**Publisher's note:** Springer Nature remains neutral with regard to jurisdictional claims in published maps and institutional affiliations.

© The Author(s), under exclusive licence to Springer Nature America, Inc. 2019

## Methods

**Vector design and construction.** One or two copies of the GluR2 adRNAs were cloned into an AAV vector containing a human U6 and mouse U6 promoter, along with a CMV promoter driving the expression of GFP or the full-length ADAR2 enzyme<sup>21–23</sup> or its hyperactive mutant ADAR2 (E488Q)<sup>24</sup>. Similarly, one or two copies of the MS2 adRNAs were cloned into an AAV vector bearing the MCP-ADAR1 or MCP-ADAR2 deaminase domain fusions and their hyperactive mutants. To construct the GFP reporters—GFP-Amber, GFP-Ochre and GFP-Opal—three gene blocks were synthesized, with ‘TAG’, ‘TAA’ and ‘TGA’, respectively, replacing the Y39 residue of the wild-type GFP, and were cloned downstream of a CAG promoter. To construct the OTC and DMD reporters, 200-bp fragments of the *spf<sup>fish</sup>* OTC and *mdx* DMD transcript bearing the target adenosine(s) to be edited were cloned downstream of the CAG promoter.

**Mammalian cell culture and transfection.** All HEK293T cells (ATCC) or HEK293FT cells (Thermo Fisher) were grown in Dulbecco’s modified Eagle’s medium supplemented with 10% fetal bovine serum and 1% antibiotic-antimycotic (Thermo Fisher) in an incubator at 37 °C and 5% CO<sub>2</sub> atmosphere. All in vitro transfection experiments were carried out using the commercial transfection reagent Lipofectamine 2000 (Thermo Fisher). All in vitro RNA editing experiments involving a reporter were carried out in 24-well plates using 400 ng of reporter plasmid and 800 ng of the adRNA + enzyme plasmid. All in vitro RNA editing experiments targeting an endogenous transcript were carried out in 24-well plates using 800 ng of the adRNA/enzyme plasmid. dCas13b-ADAR2/DDE488Q-based RNA editing experiments were carried out using 800 ng of the enzyme plasmid (Addgene, no. 103864) and 800 ng of the gRNA plasmid. Cells were transfected at 25–30% confluence and harvested 60 h post-transfection for quantification of editing. Chemically synthesized adRNAs (synthesized by either IDT or Synthego) were transfected using Lipofectamine 3000 (Thermo Fisher) at 20 pmol per well.

**Production of AAV vectors.** The AAV8 particles were produced using HEK293T cells via the triple-transfection method and purified via an iodixanol gradient. Confluency at transfection was about 80%. Two hours before transfection, Dulbecco’s modified Eagle’s medium supplemented with 10% fetal bovine serum was added to the HEK293T cells. Each virus was produced in 5 × 15 cm plates, where each plate was transfected with 7.5 μg of pXR-8, 7.5 μg of recombinant transfer vector and 7.5 μg of pHelper vector using polyethylenimine (PEI) (1 μg μl<sup>-1</sup> linear PEI in 1 × Dulbecco’s phosphate-buffered saline, pH 4.5, using hydrochloric acid) at a PEI:DNA mass ratio of 4:1. The mixture was incubated for 10 min at room temperature and then applied dropwise onto the cell media. The virus was harvested after 72 h and purified using an iodixanol density gradient ultracentrifugation method. The virus was then dialyzed with 1 × phosphate-buffered saline (pH 7.2) supplemented with 50 mM sodium chloride and 0.0001% Pluronic F68 (Thermo Fisher) using 50-kDa filters (Millipore), to a final volume of ~1 ml, and quantified by quantitative PCR using primers specific to the ITR region, against a standard (ATCC VR-1616): AAV-ITR-F, 5′-CGGCCTCAGTGAGCGA-3′; AAV-ITR-R, 5′-GGAACCCCTAGTGATGGAGTT-3′.

**RNA isolation and next-generation sequencing library preparation.** Extraction of RNA from animal tissue was done using the RNeasy Plus Universal Mini Kit (Qiagen), according to the manufacturer’s protocol. RNA from cells was extracted using the RNeasy Mini Kit (Qiagen). Complementary DNA (cDNA) was synthesized from 500 ng of RNA using the Protoscript II First Strand cDNA synthesis Kit (NEB). Next-generation sequencing libraries were prepared as follows. Briefly, 1 μl of cDNA prepared as above was amplified by PCR with primers that amplify about 150 bp surrounding the sites of interest using KAPA Hifi HotStart PCR mix (Kapa Biosystems). PCR products were purified (Qiagen PCR purification kit/gel extraction kit) to eliminate by-products. Libraries were constructed with the NEBNext Multiplex Oligos for Illumina kit (NEB). Next, 10 ng of input DNA was amplified with indexing primers. Samples were then pooled and loaded on either an Illumina MiSeq (150 bp single-end run) or HiSeq (100 bp paired-end run). Data analysis was performed using CRISPResso<sup>25</sup>. A minimum of 100,000 reads were analyzed for all in vivo experiments. RNA-seq libraries were prepared from 300 ng of RNA using the NEBNext poly(A) mRNA magnetic isolation module and NEBNext Ultra RNA library prep kit for Illumina. Samples were pooled and loaded on an Illumina HiSeq (100 bp paired-end run).

**Quantification of OTC mRNA editing yields in *spf<sup>fish</sup>* mice.** The *spf<sup>fish</sup>* mouse model has three forms of OTC RNA: pre-mRNA, the correctly spliced mRNA and an incorrectly spliced, elongated mRNA formed owing to the use of a cryptic splice site 48 bp into intron 4<sup>18</sup>. Let the total number of correctly spliced mRNA be *X*, incorrectly spliced variant be *Y* and pre-mRNA be *Z*. *X<sub>e</sub>*, *Y<sub>e</sub>* and *Z<sub>e</sub>* denote the A>G edited mRNA in the three forms. The mRNA editing yield ideally would be calculated as  $(X_e + Y_e + Z_e)/(X + Y + Z)$ . However, because it is not possible to amplify spliced and pre-mRNA variants using the same primers, in Fig. 2e we report the fraction of edited transcripts in the correctly spliced mRNA (*X<sub>e</sub>/X*), which will in turn be translated to produce the OTC protein. In addition, in Supplementary Fig. 12c we also report the fraction of edited transcripts in pre-mRNA (*Z<sub>e</sub>/Z*). This fraction, following correct splicing, will contribute to

the formation of OTC protein. Finally, incorrectly spliced mRNA results in the production of a protein elongated by 16 amino acids, which is selectively degraded. Supplementary Fig. 12d shows bands corresponding to *X* and *Y*.

**Animal experiments.** All animal procedures were performed in accordance with protocols approved by the Institutional Animal Care and Use Committee of the University of California, San Diego. All mice were acquired from Jackson Labs. AAVs were injected into either the gastrocnemius or tibialis anterior muscle of *mdx* mice (C57BL/10ScSn-*Dmd<sup>mdx</sup>/J*) using 2.5 × 10<sup>12</sup> vector genomes per muscle. AAVs were injected into *spf<sup>fish</sup>* mice (B6EiC3Sn a/A-*Otc<sup>spf-ash</sup>/J*) by retro-orbital injection using 2.5 × 10<sup>12</sup> vector genomes per mouse. Mice that appeared to have a rough hair coat, moved slowly and appeared slightly hunched were termed sick mice and were euthanized.

**Immunofluorescence.** Harvested gastrocnemius or tibialis anterior muscles were placed in molds containing OCT compound (VWR) and flash-frozen in liquid nitrogen. Sections of 10 μm were cut onto pretreated histological slides. Slides were fixed using 4% paraformaldehyde. Dystrophin and nNOS were detected with rabbit polyclonal antibodies against the C-terminal domain of dystrophin (1:200, Abcam, No. 15277) and the N-terminal domain of nNOS (1:100, Immunostar, No. 24431), respectively, followed by donkey anti-rabbit Alexa Fluor 546 secondary antibody (1:400, Thermo Fisher).

**Immunoblots.** Muscle biopsies from *mdx* mice and liver biopsies from *spf<sup>fish</sup>* mice were fragmented in RIPA buffer (Sigma) with a proteinase inhibitor cocktail (Roche) and incubated for 1 h on ice with intermittent vortexing. Samples were centrifuged at 15,500g for 30 min at 4 °C, and the supernatant was isolated and quantified with a Pierce Coomassie Plus (Bradford) assay kit (Thermo Fisher). Protein isolate was mixed with 4 × Laemmli loading buffer (Bio-Rad) and 2-mercaptoethanol (Bio-Rad) and boiled at 100 °C for 10 min. Total protein (100 μg) from muscle biopsies or 60 μg from liver biopsies was loaded into each well of a 4–15% Mini Protean TGX gel (Bio-Rad) with Tris–glycine–SDS buffer (Bio-Rad) and electrophoresed for 60 min at 100 V. Protein from muscle biopsies was transferred to nitrocellulose membranes overnight at 34 V, while that from liver biopsies was transferred at 65 V for 1 h 30 min in a 1 × Tris–glycine transfer buffer containing 10% methanol and 0.1% SDS at 4 °C. The blot was blocked for 1 h in 5% milk–Tris–buffered saline with Tween (TBST). Blots were probed with rabbit anti-dystrophin (1:200, Abcam, no. 15277), rabbit anti-GAPDH (1:4,000, Cell Signaling, no. 2118S), rabbit anti-OTC (1:800, Abcam, no. 203859) and mouse anti-ADAR2 (1:150, Santa Cruz Biotechnology, no. 73409) overnight at 4 °C in 5% milk–TBST. Blots were washed with TBST and then incubated with anti-rabbit or anti-mouse horseradish-peroxidase-conjugated secondary antibodies (Cell Signaling) for 1 h in 5% milk–TBST. After being washed with TBST, blots were visualized with SuperSignal West Femto Chemiluminescent Substrate (Thermo Fisher) and radiography.

**Statistics and reproducibility.** *In vitro* experiments. All in vitro experiments were carried out once with a minimum of three independent replicates.

*In vivo* experiments. For the *mdx* mouse model, ADAR2 and MCP-ADAR1 (E1008Q) NLS-based experiments were carried out twice. Both rounds of experiments yielded consistent RNA editing efficiencies, dystrophin immunofluorescence and dystrophin restoration as seen by immunoblots. ADAR2 (E488Q)- and CRISPR-Cas9-based experiments were carried out once. For the *spf<sup>fish</sup>* mouse model, all experiments were carried out twice, based on the availability of mice. RNA editing efficiencies of the OTC transcript, both spliced and pre-mRNA, were consistent in both rounds of experiments. RT-PCR and immunoblots were carried out on all animals in experimental set 1.

**Quantification of RNA A>G editing.** *RNA-seq read alignment.* RNA-seq read pairs with 100 bases per read mate were aligned to the GRCh38 reference genome using STAR aligner version 2.6.0c (ref. 26). The genome index was built using primary assembly annotations from GENCODE release 28 (GRCh38.p12). Default parameters were used to run STAR, except for the following relevant settings: readMapNumber = -1, alignSJoverhangMin = 5, alignSJBoverhangMin = 1, alignEndsType = EndToEnd, outFilterMismatchNmax = 10, outFilterMultimapNmax = 1, outSAMunmapped = 0, outSAMmultNmax = 1. The reads of the resulting uniquely aligned pairs were sorted by genomic coordinates using samtools sort<sup>27</sup>. Duplicated read pairs were marked using samtools markdup and were removed from subsequent analysis. Tallies of total, aligned, duplicated and remaining reads (not pairs) are reported for each sample in Supplementary Table 3.

*Selection of reference sites for quantification of editing yields.* The assessment of sites with significant changes in A-to-G editing yields (see below) is sensitive to the number of uniquely aligned reads available for each sample. To minimize potential biases when comparing different samples in terms of significantly edited sites, the uniquely aligned reads for each HEK293T sample were down-sampled using samtools view with option -s, and the down-sampling fractions are reported

in Supplementary Table 3. We calculated these fractions by dividing the lowest number of uniquely aligned reads among all samples by the number of uniquely aligned reads available for the sample being down-sampled. Down-sampling was not performed on the reads of the control sample, the first in Supplementary Table 3. The down-sampled reads were then processed using samtools mpileup. The output of this tool was parsed to extract the counts of each base found in the aligned reads at each A and T site in the GRCh38 reference genome sequence. Insertions and deletions were ignored. Reference sites with read coverage < 10 were omitted from downstream analysis. The number of remaining reference A and T sites with read coverage  $\geq 10$  varied by  $\sim 15\%$  across the samples listed in Supplementary Table 3. Without down-sampling, this number was found to vary by  $\sim 50\%$ . From the reference A and T sites with read coverage  $\geq 10$ , we selected a final list of total sites (A and T sites) by choosing those sites that were common to all samples and for which at least one G or C was observed at a reference A or T site, respectively, in the aligned reads of at least one sample. The other sites, those not common to all samples or with zero observed editing events in all samples, were discarded.

**Assessment of significant changes in A-to-G editing yields.** To uncover significant changes in A-to-G editing yields, we considered several pairs of control and treatment samples. For each pair, the control sample was the first sample listed in Supplementary Table 3, and the treatment sample was one of the samples shown in Fig. 1. For each pair of compared samples, and for each reference A site selected as described above, a Fisher exact test was carried out using a  $2 \times 2$  contingency matrix C with entries defined as follows:  $C_{1,1}$  = count of bases other than G observed in the control sample;  $C_{2,1}$  = count of G bases observed in the control sample;  $C_{1,2}$  = count of bases other than G observed in the test sample; and  $C_{2,2}$  = count of G bases observed in the test sample. A similar contingency matrix was used for each selected reference T site, except that G was replaced with C in the above definitions. The P values calculated for all selected reference sites and for a given comparison of samples were adjusted for multiple testing using the Benjamini–Hochberg method. A and T sites with adjusted P values less than an FDR of 1% and with a fold change of at least 1.1 in editing yield were

deemed to have a significant change in A-to-G editing yield on forward and reverse transcripts, respectively. The counts of these sites for each comparison of samples are shown as  $N_{\text{sig}}$  in Supplementary Fig. 7, and are reported under the column ‘changed sites’ in Supplementary Table 4. The total number of reference sites with a significant change in A-to-G editing yield was computed. The editing yields at these sites were used to construct the distributions shown in Fig. 1c. The on-target A-to-G editing yields shown as blue circles in Fig. 1c and Supplementary Fig. 7 were estimated for each sample as  $C_{2,2}/(C_{1,2} + C_{2,2})$  using counts observed at the intended target A site in the RAB7A transcript. These values are reported under the column ‘editing yield’ in Supplementary Table 4. The 1-based genomic coordinate of the intended target A site was found to be chr3:128814202 after submission of the following sequence to BLAT after selection of reference assembly hg38: AGCGGCAGTATTCTGTACAGTAGACA CAAGAATTATGTACGCCTTTATCA.

**Reporting Summary.** Further information on research design is available in the Nature Research Reporting Summary linked to this article.

### Data availability

Data are accessible via the NCBI GEO under accession [GSE123905](#), and also are available from the corresponding author upon reasonable request. Source data for Figs. 1 and 2 and for Supplementary Figs. 1–6 and 10–13 are available online.

### References

21. Bass, B. L. & Weintraub, H. *Cell* **55**, 1089–1098 (1988).
22. Ohman, M., Källman, A. M. & Bass, B. L. *RNA* **6**, 687–697 (2000).
23. Lehmann, K. A. & Bass, B. L. *Biochemistry* **39**, 12875–12884 (2000).
24. Matthews, M. M. et al. *Nat. Struct. Mol. Biol.* **23**, 426–433 (2016).
25. Pinello, L. et al. *Nat. Biotechnol.* **34**, 695–697 (2016).
26. Dobin, A. et al. *Bioinformatics* **29**, 15–21 (2013).
27. Li, H. et al. *Bioinformatics* **25**, 2078–2079 (2009).

## Reporting Summary

Nature Research wishes to improve the reproducibility of the work that we publish. This form provides structure for consistency and transparency in reporting. For further information on Nature Research policies, see [Authors & Referees](#) and the [Editorial Policy Checklist](#).

### Statistical parameters

When statistical analyses are reported, confirm that the following items are present in the relevant location (e.g. figure legend, table legend, main text, or Methods section).

n/a Confirmed

- The exact sample size ( $n$ ) for each experimental group/condition, given as a discrete number and unit of measurement
- An indication of whether measurements were taken from distinct samples or whether the same sample was measured repeatedly
- The statistical test(s) used AND whether they are one- or two-sided  
*Only common tests should be described solely by name; describe more complex techniques in the Methods section.*
- A description of all covariates tested
- A description of any assumptions or corrections, such as tests of normality and adjustment for multiple comparisons
- A full description of the statistics including central tendency (e.g. means) or other basic estimates (e.g. regression coefficient) AND variation (e.g. standard deviation) or associated estimates of uncertainty (e.g. confidence intervals)
- For null hypothesis testing, the test statistic (e.g.  $F$ ,  $t$ ,  $r$ ) with confidence intervals, effect sizes, degrees of freedom and  $P$  value noted  
*Give  $P$  values as exact values whenever suitable.*
- For Bayesian analysis, information on the choice of priors and Markov chain Monte Carlo settings
- For hierarchical and complex designs, identification of the appropriate level for tests and full reporting of outcomes
- Estimates of effect sizes (e.g. Cohen's  $d$ , Pearson's  $r$ ), indicating how they were calculated
- Clearly defined error bars  
*State explicitly what error bars represent (e.g. SD, SE, CI)*

Our web collection on [statistics for biologists](#) may be useful.

### Software and code

Policy information about [availability of computer code](#)

Data collection

No software was used

Data analysis

RNA-seq data were analyzed using samtools, pysam version 0.15.1, R version 3.5.1, ggplot2 version 3.1.0 and DESeq version 1.34.0, python version 2.7.15, perl version 5.22.2, STAR version 2.5.3a, STAR version 2.6.0c.  
STAR aligner, Dobin, A. et al. STAR: ultrafast universal RNA-seq aligner. *Bioinformatics* 29, 15–21 (2013).  
SAMtools version, Li, H. et al. The Sequence Alignment/Map format and SAMtools. *Bioinformatics* 25, 2078–2079 (2009).  
DESeq, Love MI. et al. Moderated estimation of fold change and dispersion for RNA-seq data with DESeq2. *Genome Biol.* 15(12):550 (2014).  
Amplicon sequencing was analyzed using CRISPResso version 1.0.13.  
CRISPResso, Pinello, L. et al. Analyzing CRISPR genome-editing experiments with CRISPResso. *Nat. Biotechnol.* 34, 695–697 (2016).  
GraphPad Prism version 7.01 was used for plotting figures.  
CellQuest Pro version 4.0.1 was used to analyze FACS data.

For manuscripts utilizing custom algorithms or software that are central to the research but not yet described in published literature, software must be made available to editors/reviewers upon request. We strongly encourage code deposition in a community repository (e.g. GitHub). See the Nature Research [guidelines for submitting code & software](#) for further information.

## Data

Policy information about [availability of data](#)

All manuscripts must include a [data availability statement](#). This statement should provide the following information, where applicable:

- Accession codes, unique identifiers, or web links for publicly available datasets
- A list of figures that have associated raw data
- A description of any restrictions on data availability

Accession codes will be available before publication. A full code availability statement is included in the manuscript.

## Field-specific reporting

Please select the best fit for your research. If you are not sure, read the appropriate sections before making your selection.

Life sciences  Behavioural & social sciences  Ecological, evolutionary & environmental sciences

For a reference copy of the document with all sections, see [nature.com/authors/policies/ReportingSummary-flat.pdf](https://www.nature.com/authors/policies/ReportingSummary-flat.pdf)

## Life sciences study design

All studies must disclose on these points even when the disclosure is negative.

Sample size	At least 3 independent samples per tested condition were evaluated.
Data exclusions	No data was excluded.
Replication	3 or more independent biological replicates were evaluated for both in vitro studies in cultured cells, and in vivo studies using mice. Findings were consistent in all replicates.
Randomization	Mice were randomly assigned into groups prior to injection.
Blinding	No blinding was carried out.

## Reporting for specific materials, systems and methods

### Materials & experimental systems

n/a	Involved in the study
<input checked="" type="checkbox"/>	<input type="checkbox"/> Unique biological materials
<input type="checkbox"/>	<input checked="" type="checkbox"/> Antibodies
<input type="checkbox"/>	<input checked="" type="checkbox"/> Eukaryotic cell lines
<input checked="" type="checkbox"/>	<input type="checkbox"/> Palaeontology
<input type="checkbox"/>	<input checked="" type="checkbox"/> Animals and other organisms
<input checked="" type="checkbox"/>	<input type="checkbox"/> Human research participants

### Methods

n/a	Involved in the study
<input checked="" type="checkbox"/>	<input type="checkbox"/> ChIP-seq
<input type="checkbox"/>	<input checked="" type="checkbox"/> Flow cytometry
<input checked="" type="checkbox"/>	<input type="checkbox"/> MRI-based neuroimaging

## Antibodies

Antibodies used

The antibodies used in this study include:  
 Rabbit anti-dystrophin (Immunofluorescence and western blot 1:200), abcam 15277, Lot no. GR 305946-5  
 Rabbit anti-nNOS (Immunofluorescence 1:100), Immunostar 24431, Lot no. 401001  
 Rabbit anti-Ornithine Carbamoyltransferase (Western blot 1:800), abcam 203859, Lot no. GR 278002-5  
 Rabbit anti-GAPDH (Western blot 1:4000), Cell Signaling 2118S, Lot no. 10  
 Mouse anti-ADAR2 (Western blot 1:150), Santa Cruz Biotechnology 73409, Lot no. K0917  
 Donkey anti-rabbit AlexaFluor 546 (Immunofluorescence 1:400), ThermoFisher A10040, Lot no. 1833519  
 Anti-rabbit IgG HRP-linked (Western blot 1:20,000), Cell Signaling 7074S, Lot no. 26  
 Anti-mouse IgG HRP-linked (Western blot 1:20,000), Cell Signaling 7076P2, Lot no. 32

Validation

Antibodies were validated and optimized by immunostaining and/or western blots carried out on tissue samples harvested from positive and negative control mice, simultaneously, as per the manufacturers instructions. The antibodies against dystrophin,

nNOS, OTC and GAPDH were validated for the mouse proteins. The antibody against ADAR2 was validated for the human protein.

References:

1. Nelson, C. E. et al. In vivo genome editing improves muscle function in a mouse model of Duchenne muscular dystrophy. *Science* (80-. ). 351, (2016).

2. Tabebordbar, M. et al. In vivo gene editing in dystrophic mouse muscle and muscle stem cells. *Science* (80-. ). 351, 407–411 (2016).

## Eukaryotic cell lines

Policy information about [cell lines](#)

Cell line source(s)	HEK293T, HEK293FT, HeLa (ATCC)
Authentication	STR, by vendor
Mycoplasma contamination	Tested by vendor, no mycoplasma contamination
Commonly misidentified lines (See <a href="#">ICLAC</a> register)	HEK293T cells were used for cell culture experiments, and AAV production per established procedures.

## Animals and other organisms

Policy information about [studies involving animals](#); [ARRIVE guidelines](#) recommended for reporting animal research

Laboratory animals	Laboratory mice used in this study were obtained from the Jackson Laboratory C57BL/10ScSn-Dmmdmx/J, strain 001801, male and female, 6-10 weeks B6EiC3Sn a/A-Otscpf-ash/J, strain 001811, male, 10-16 weeks
Wild animals	Study did not involve wild animals.
Field-collected samples	Study did not involve samples collected from the field.

## Flow Cytometry

Plots

Confirm that:

- The axis labels state the marker and fluorochrome used (e.g. CD4-FITC).
- The axis scales are clearly visible. Include numbers along axes only for bottom left plot of group (a 'group' is an analysis of identical markers).
- All plots are contour plots with outliers or pseudocolor plots.
- A numerical value for number of cells or percentage (with statistics) is provided.

Methodology

Sample preparation	The HEK293T cell line was used for all flow cytometry experiments. Flow cytometry was carried out on the transfected cells 48 or 72 hours post transfection to quantify GFP expression. No antibodies were used for flow cytometry.
Instrument	FACScan (Becton Dickinson)
Software	CellQuest Pro (Becton Dickinson)
Cell population abundance	n/a
Gating strategy	Un-transfected control cells were used to define non-fluorescent cells (with a gating boundary defined at a fluorescence intensity of $10^1$ ).

- Tick this box to confirm that a figure exemplifying the gating strategy is provided in the Supplementary Information.